Biophysical Journal
Article

Biophysical Society

At sixes and sevens: cryptic domain in the metal binding chain of the human copper transporter ATP7A

Eva-Maria E. Uhlemann,[1] Woonghee Lee,[2] Marco Tonelli,[3] and Oleg Y. Dmitriev[1,*]
[1]Department of Biochemistry, Microbiology and Immunology, University of Saskatchewan, Saskatoon, Saskatchewan, Canada; [2]Department of Chemistry, University of Colorado, Denver, Colorado; and [3]National Magnetic Resonance Facility at Madison, University of Wisconsin, Madison, Wisconsin

ABSTRACT ATP7A and ATP7B are structurally similar but functionally distinct active copper transporters that regulate copper levels in the human cells and deliver copper to the biosynthetic pathways. Both proteins have a chain of six cytosolic metal-binding domains (MBDs) believed to be involved in the copper-dependent regulation of the activity and intracellular localization of these enzymes. Although all the MBDs are quite similar in structure, their spacing differs markedly between ATP7A and ATP7B. We show by NMR that the long polypeptide between MBD1 and MBD2 of ATP7A forms an additional seventh metastable domain, which we called HMA1A (heavy metal associated domain 1A). The structure of HMA1A resembles the MBDs but contains no copper-binding site. The HMA1A domain, which is unique to ATP7A, may modulate regulatory interactions between MBD1–3, contributing to the distinct functional properties of ATP7A and ATP7B.

SIGNIFICANCE Human copper transporters ATP7A and ATP7B control copper levels in the cell and assist in incorporating copper as a cofactor into maturing metalloproteins. Mutations in ATP7A and ATP7B cause severe disorders of copper metabolism, Menkes disease and Wilson disease, respectively. Enzymatic activity and intracellular localization of ATP7A and ATP7B are regulated by copper through the complex dynamics of the chain of six highly mobile metal-binding domains. We have identified a new and, to our knowledge, previously uncharacterized metastable domain within this chain in ATP7A and solved its structure by NMR. The new domain, HMA1A (heavy metal associated domain 1A), which is absent from ATP7B, may participate in the regulation of ATP7A activity and serve as a structural determinant of the major functional distinctions between the two human copper transporters.

INTRODUCTION

Copper is an essential but potentially toxic biometal (1) that readily interacts with proteins and enters damaging chemical reactions in the cell. To control biochemical fate of copper, the metal is delivered to its intracellular destinations and excreted from the cell along complex specialized pathways that involve many interacting proteins. The two active copper transporters ATP7A and ATP7B receive copper from the cytosolic chaperone ATOX1 and then translocate it across the cell membranes for incorporation into the newly synthesized proteins as a cofactor or for excretion of the excess copper from the cell.

ATP7A and ATP7B are structurally very similar proteins, with ~60% amino acid residue sequence identity, belonging to the large family of P-type ATPases. The copper ATPases share much of the domain structure and the fundamental features of the catalytic mechanism with the better studied members of the family, such as Ca^{2+}-ATPase and Na^{+},K^{+}-ATPase (2–8). A unique structural feature of ATP7A and ATP7B is the N-terminal chain of six metal-binding domains (MBDs) located in the cytosol (Fig. 1 *A*). Each domain is ~70 amino acids long and has a conserved ferredoxin-like fold with the invariant dicysteine (CxxC) motif, which binds copper (9,10).

In contrast to their structural similarity, tissue distribution, functional roles, and regulation of ATP7A and ATP7B are rather different (12). Although both enzymes

Submitted May 18, 2021, and accepted for publication August 25, 2021.

*Correspondence: oleg.dmitriev@usask.ca

Eva-Maria E. Uhlemann and Woonghee Lee contributed equally to this work.

Editor: Timothy Cross.

https://doi.org/10.1016/j.bpj.2021.08.029

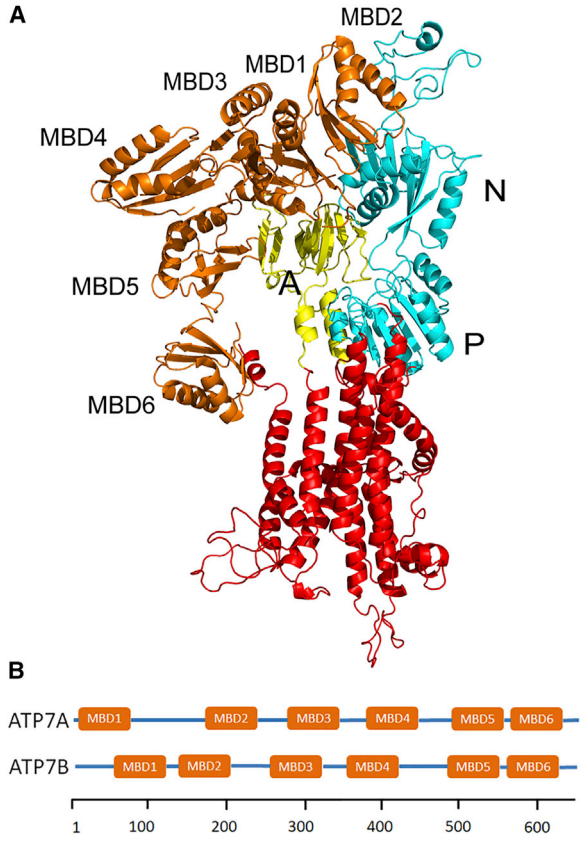

FIGURE 1 The MBD chains in human copper ATPases. (*A*) A composite model of the human copper transporter ATP7A. The MBDs (MBD1–MBD6) are in orange, the ATP-binding domain comprising the nucleotide binding (N) and phosphorylation (P) domains is in cyan, the actuator (A) domain is in yellow, and the transmembrane domain is in red. The model, excluding the MBDs, was generated using Robetta. The NMR structures of the individual MBDs were positioned manually based on the previously published models (11). (*B*) Spacing of the MBDs in the human copper transporters ATP7A and ATP7B. Residue number scale is shown below. To see the figure in color, go online.

participate in copper delivery to the biosynthetic pathways, ATP7B appears to be particularly important for the removal of excess copper by excreting it from hepatocytes into the bile. ATP7A, on the other hand, is required for copper uptake in the intestine, where it transports copper across the basolateral membrane of enterocytes into the bloodstream. These distinct physiological functions result in either severe copper deficiency or, conversely, copper toxicosis when ATP7A or ATP7B is impaired by mutations in Menkes disease or Wilson disease, respectively.

At the basal copper levels in the cell, ATP7B and ATP7A are located in the *trans*-Golgi network, where they deliver copper to the maturing copper-containing proteins. As the copper level in the cell increases, both proteins relocate to the cytosolic membrane vesicles and to the plasma membrane and export copper from the cell (13,14). In polarized cells, ATP7B is usually found in the apical membrane and ATP7A in the basolateral membrane. Thus regulation of copper transporters is rather complex and involves both the enzyme turnover rate and protein trafficking.

The mechanism of regulation of copper ATPases activity and intracellular localization is still mostly a subject of hypotheses. Several lines of evidence suggest that the N-terminal chain of six MBDs plays the main role in the copper-dependent regulation of ATP7A and ATP7B. Domain truncations and mutational inactivation of the copper-binding sites in ATP7B showed that either MBD5 or MBD6 is required for copper transport (15,16), whereas only MBD6 was required for copper-dependent trafficking to the cytoplasmic vesicles. The first three MBDs could not functionally replace MBD4–6 (15). MBD1–4 have been proposed to regulate copper transport and trafficking of ATP7B by gating copper access to MBD5 and MBD6 (17). Thus, MBD5 and -6, which are closest to the membrane, are believed to be involved in the copper transfer to the transmembrane site, whereas MBD1–4 play a regulatory role.

NMR shows that the MBD1–6 chains in both ATP7B and ATP7A do not fold into stable compact structures, and the individual MBDs experience a large degree of independent mobility restricted by the flexible interdomain linkers of various length (18–20). However, in ATP7B, MBD5–6 interact with each other (21), and MBD1–3 form a dynamically correlated domain group because of the relatively weak interactions between MBD1 and MBD3 (22). MBD4 does not appear to interact with the other domains and likely serves as a structural link between the two domain groups. Biochemical data support interactions between the MBDs (23–26). Copper transfer from ATOX1 breaks up MBD1–3 interactions, increasing domain mobility (11). A structure-based mechanism of ATP7B regulation through transient domain interactions and copper-dependent dynamics of MBD1–3 has been proposed (11,27).

Differences between the functional roles of ATP7A and ATP7B suggest distinct features of the regulation mechanisms in these two enzymes, and the MBD chains in ATP7B and ATP7A show notable differences in domain spacing, even though all the individual MBDs share high sequence and structural similarity. One major difference between ATP7A and ATP7B is the length of the connecting segment between MBD1 and MBD2. In ATP7A, MBD1 and MBD2 are separated by 95 amino acid residues (H76–V171), whereas in ATP7B, the MBD1-MBD2 linker is less than 20 amino acids long (Fig. 1 *B*). Such a major difference in the linker length should have a major effect on the dynamic properties of the first three MBDs and, consequently, on the regulation of ATP7A and ATP7B. Moreover, sequence analysis of the MBD chain of ATP7A, e.g., by ScanProsite (28), shows a weak match for an additional heavy-metal-associated domain including residues I103–E152. We have investigated the structure of the region between MBD1 and MBD2 of ATP7A by NMR and discovered, to our knowledge, a new metastable domain that has a ferredoxin-like

fold, similar to the previously known MBDs, but lacks a copper-binding site. We propose that reversible folding and unfolding of this domain is involved in the regulation of ATP7A activity.

MATERIALS AND METHODS

Protein expression and purification

DNA sequence encoding residues 76–170 of ATP7A were codon optimized for *Escherichia coli* expression and prepared by chemical synthesis (GenScript, Piscataway, NJ). The ATP7A$_{76–170}$ and HMA1A(heavy metal associated domain 1A) protein constructs were expressed as fusions with the chitin-binding domain and intein using vector pTYB12 (New England Biolabs, Ipswich, MA). ATP7A$_{76–170}$ was expressed in *E. coli* strain BL21(DE3). HMA1A expression and purification was tested in *E. coli* BL21(DE3) and in three strains coexpressing various folding chaperones, BL21(DE3)-pG-KJE7 (TaKaRa Bio, Mountain View, CA) coexpressing *dnaK*, *dnaJ*, and *grpE*; BL21Gold (DE3)/pTf16 (TaKaRa Bio) coexpressing the *tig* trigger factor; and ArcticExpress (DE3) (Agilent Technologies, Santa Clara, CA) coexpressing *cpn10* and *cpn60* from *Oleispira antarctica*. The proteins were isotopically labeled with ^{15}N and ^{13}C and purified by chitin affinity chromatography combined with intein self-cleavage, essentially as described previously (29), except that HMA1A expression was induced in ArcticExpress (DE3) cells (Agilent Technologies) in the M9 medium by adding 0.5 mM isopropylthio-β-galactoside, followed by incubation at 10°C for 24 h. HMA1A was additionally purified by size-exclusion chromatography on a Superdex 75 10/300 GL Increase column (GE Life Sciences, Marlborough, MA) in a buffer containing 50 mM HEPES-Na (pH 7.4), 150 mM NaCl, and 5 mM *tris*-(2-carboxyethyl)phosphine and concentrated by membrane filtration.

NMR experiments and structure determination

NMR samples contained 0.1–0.2 mM protein in 50 mM HEPES-Na (pH 7.4), 150 mM NaCl, 5 mM tris(2-carboxyethyl)phosphine, 5% v/v $^{2}H_2O$, and 0.25 mM 2,2-dimethyl-2-silapentane-5-sulfonate. Data for HMA1A backbone chemical shift assignment and structure determination, including two-dimensional heteronuclear single quantum coherence spectra (^{1}H,^{15}N-HSQC,) three-dimensional (3D) HNCA, 3D HNCACB, 3D CBCA(CO)NH, and 3D NOESY-^{15}N-HSQC spectra, were collected with a uniformly ^{13}C,^{15}N-labeled sample on a 600-MHz Bruker Avance III spectrometer (Billerica, MA) equipped with a cryogenic triple-resonance probe at a sample temperature of 298 K. To reduce the acquisition time, all 3D spectra were recorded using nonuniform sampling with a sampling rate of 32%, with the exception of the 3D NOESY, which was recorded using a sampling rate of 36%.

NMRPipe (30) and SMILE packages were used to process and reconstruct the nonuniform sampling data (31). The automation and visual verification plugins in NMRFAM-SPARKY were used to obtain resonance chemical shifts (32). Peaks in two-dimensional ^{1}H,^{15}N-HSQC, 3D HNCA, 3D HNCACB, and 3D CBCA(CO)NH spectra were picked with the automated peak-picking program APES and inspected via strip plots (33). The initial assignments were obtained using the I-PINE web server (http://i-pine.nmrfam.wisc.edu) with PINE-SPARKY.2 plugin (34,35) and then verified visually with the help of PINE-SPARKY plugins PINE Graph and PINE Assigner (34).

To obtain the 3D structure of HMA1A, we employed a method combining chemical shift-based structure prediction with sparse restraint structure calculation. The initial fold was calculated on the Biological Magnetic Resonance Data Bank CS-Rosetta web server (https://csrosetta.bmrb.io) with 10,000 starting structures. The best structure from CS-Rosetta was used as input to Ponderosa Client to assist 3D-NOESY assignments by AUDANA algorithm and generate distance restraints using PONDEROSA-C/S package (36–39). As a final step, we used Xplor-NIH software with the generated distance, angle, and hydrogen bond restraints to calculate and refine 2000 structures. The 20 best structures, based on the lowest energy criteria, were additionally refined in a TIP3P water model box (40). Secondary structure was detected using STRIDE software tool (41). Structure quality was evaluated with Protein Structure Validation Software (PSVS) 1.5 (42). The final structure ensemble has been deposited in the Worldwide Protein Data Bank (43) (PDB: 7LU8). The associated chemical shift data have been deposited in the Biological Magnetic Resonance Data Bank (44) (BMRB: 30866).

RESULTS AND DISCUSSION

We have first expressed and purified the entire fragment connecting MBD1 and MBD2 of ATP7A (Fig. 1), including residues H76–E170 (ATP7A$_{76–170}$). The protein was expressed as a fusion with the chitin-binding domain and intein and purified by chitin affinity chromatography combined with thiol-induced intein self-cleavage. The ^{1}H,^{15}N-HSQC spectrum of ATP7A$_{76–170}$ revealed a largely disordered protein (Fig. 2 *A*). However, a pattern of small but narrow and well-dispersed peaks indicated the presence of a well-folded domain in a fraction of the protein, with an

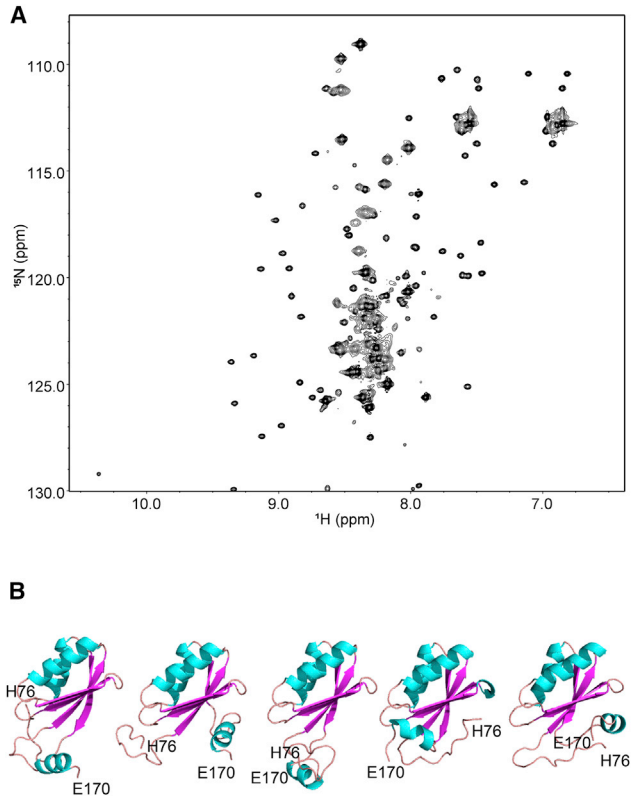

FIGURE 2 Structural propensity of the polypeptide connecting the first two MBDs of ATP7A. (*A*) A ^{1}H,^{15}N-HSQC spectrum of the protein fragment corresponding to the complete region between MBD1 and MBD2 (ATP7A$_{76–170}$). (*B*) The top five structure models of ATP7A$_{76–170}$ predicted by Robetta, with the N- and C-terminal residues labeled and the α-helices shown in *aquamarine*, β-strands in *magenta* and loop regions in *salmon*. To see the figure in color, go online.

estimated size of 50–70 amino acid residues, similar to the size of the MBDs in ATP7A.

Unlike the MBDs, $ATP7A_{76–170}$ does not contain the copper-binding CxxC motif and does not interact with the copper chaperone ATOX1 in either copper-free, or copper-bound form (Fig. S1). To determine the location of the folded core in the $ATP7A_{76–170}$ sequence, we performed *ab initio* structure modeling with Robetta (45). The top five models consistently showed a characteristic ferredoxin fold encompassing residues 85–156 (Fig. 2 *B*). Residues 76–84 were disordered, and residues 157–185 included a loop region and a short (1.5–2 turns), randomly oriented α-helix.

We then expressed and purified the ATP7A fragment encompassing residues 85–156. The standard expression procedure in BL21(DE3) strain yielded a mostly disordered protein (Fig. S2 *A*). Expression in the strains producing various chaperone proteins significantly improved protein folding (Fig. S2, *B–D*). The best results were obtained using protein expression at a low temperature in the ArcticExpress strain, which also expresses chaperonins Cpn10 and Cpn60 from the psychrophilic bacterium *Oleispira antarctica*. Additional purification by size-exclusion chromatography produced a well-folded monomeric protein (Fig. 3 *A*), which we designated HMA1A to emphasize its predicted fold and to distinguish it from the neighboring functional MBDs, MBD1 and MBD2.

Our attempts to crystallize HMA1A were unsuccessful, and its propensity to aggregate in a time-dependent manner at higher protein concentrations prevented structure determination by the conventional protein NMR approach, which requires complete chemical shift and NOE assignment. Nevertheless, we were able to make the backbone chemical shift assignments of HMA1A (Fig. 3 *A*) from HNCA, HNCACB, and CBCA(CO)NH experiments and to record a 3D $^{1}H,^{15}N$-HSQC-NOESY spectrum. From these data, we have determined the HMA1A structure using chemical shift-based and sparse restraint structure calculation methods (Table S1). This method is sufficiently robust to accurately determine the global fold of HMA1A, but additional NOE restraints, beyond those between the backbone amide protons, would be required to achieve higher resolution and improve reliability of the structure details.

The HMA1A structure shows a $\beta\alpha\beta\beta\alpha$-fold, rather similar to the ferredoxin archetype-$\beta\alpha\beta\beta\alpha\beta$, but with the segment corresponding to β4 in a disordered state (Fig. 3 *B*; Fig. S3). Overall, the HMA1A structure is quite similar to the adjacent MBD1 (46) and MBD2 (47) (Fig. 3 *C*), even though the sequence of HMA1A does not show any significant homology to the MBDs, which are quite similar among themselves (Fig. S4). The experimentally determined HMA1A structure is also quite similar to the top Robetta models, with the main difference found in the C-terminal region, where Robetta predicts a short β-strand comprising residues D149–T152 (Fig. S5).

Alignment of the ATP7A sequences across various animal taxa does not reveal any universally conserved motifs in the region corresponding to HMA1A in the human ATP7A that could give a clue to HMA1A function, but there are several regions of relatively high sequence conservation, notably residues 111–117 and 127–132, which include parts of the β2 and β3 strands and the adjacent loops (Fig. 4 *A*).

Over the course of evolution, divergence of a single active copper transporter into ATP7A and ATP7B appears to have first occurred in chordates (48). To test if HMA1A is a salient

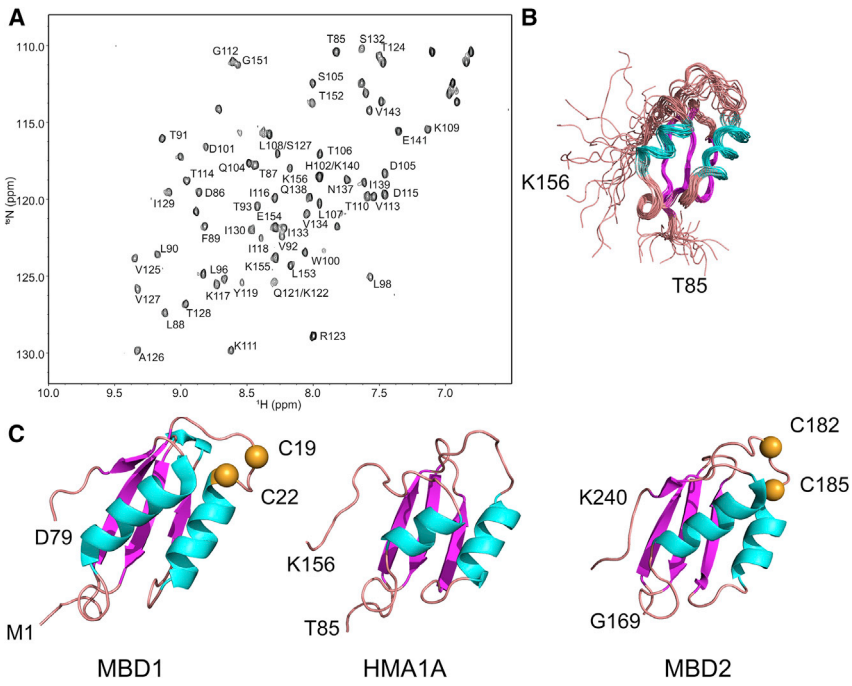

FIGURE 3 NMR structure determination of HMA1A. (*A*) A $^{1}H,^{15}N$-HSCQC spectrum of HMA1A with the sequential residue assignments shown. Residue numbering corresponds to the full-length protein. (*B*) The 20 lowest energy structures of HMA1A with the N- and C-terminal residues labeled. (*C*) Structures of MBD1, HMA1A, and MBD2 of ATP7A. The N- and C-terminal residues are labeled, and the α-helices are shown in *aquamarine*, β-strands in *magenta* and loops in *salmon*.The cysteine residues in the copper-binding CxxC motifs in MBD1 (PDB: 1KVI) and MBD2 (PDB: 1S6O) are shown as orange spheres and labeled. To see the figure in color, go online.

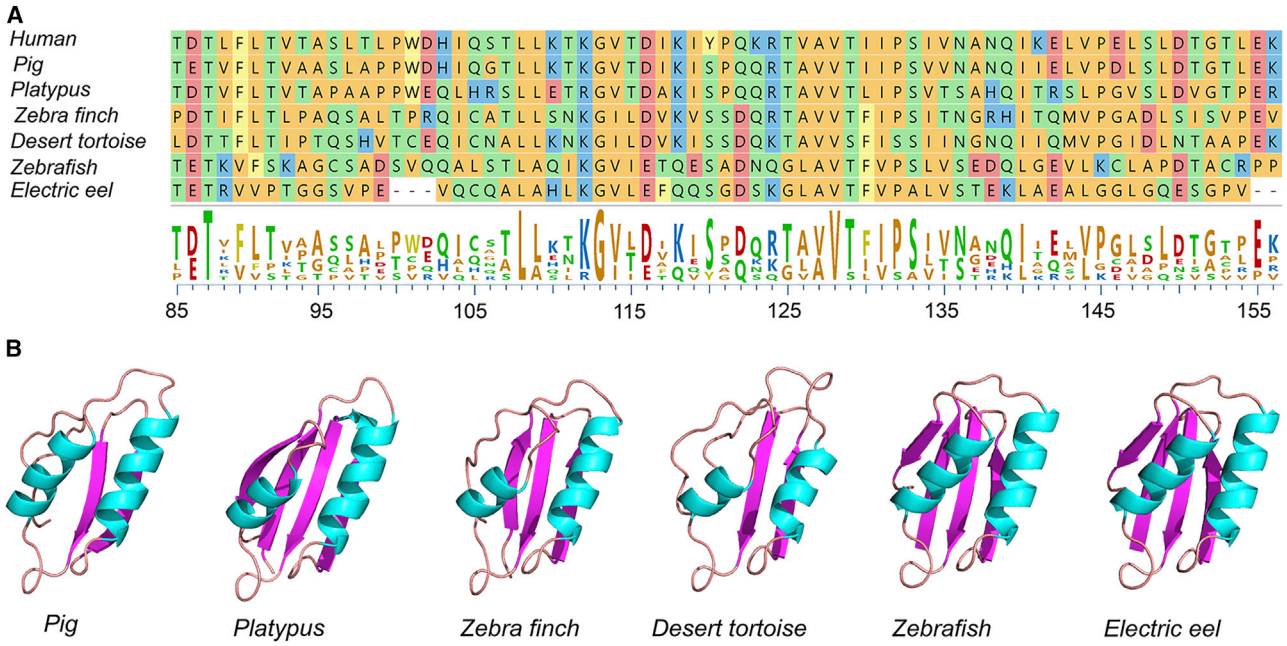

FIGURE 4 Sequence alignment (*A*) and structure models (*B*) of the regions corresponding to the human HMA1A in various species. Amino acid residue variability is shown below the alignment. The structure models were calculated using Robetta. The α-helices are shown in *aquamarine*, β-strands in *magenta* and loops in *salmon*.To see the figure in color, go online.

structural feature of ATP7A proteins from evolutionary distant species, we have performed a Robetta structure prediction on the sequences corresponding to the human HMA1A in ATP7A from several species randomly chosen from various vertebrate taxa, including the domestic pig (*Sus scrofa*), platypus (*Ornithorhynchus anatinus*), Agassiz's desert tortoise (*Gopherus agassizii*), zebra finch (*Taeniopygia guttata*), zebrafish (*Danio rerio*), and the electric eel (*Electrophorus electricus*). Although these sequences share only four identical residues (sequence identity 6%), all of them form rather similar predicted folds (Fig. 4 *B*). This finding suggests that HMA1A is not just a vestige of the multiple gene duplication and recombination events that were likely involved in the formation of the chain of the MBDs in the copper transporters during evolution but may have a defined functional or structural role. It also indicates that the protein fold rather than a specific sequence motif defines the function of HMA1A.

The high content of disordered protein in the initial preparations (Fig. S2 *A*) suggested that the HMA1A domain is unstable. We have tested thermal stability of HMA1A (Fig. 5 *A*) in comparison with the MBD2 of ATP7B (Fig. 5 *B*), monitoring the peak volume of the amino acid residue signals of the folded form of the protein (Fig. 5 *C*).

MBD2 unfolded as a single unit with a melting temperature of ∼330 K (57°C) (Fig. 5 *D*). The protein largely refolded upon cooling the sample back to 298 K (25°C), as shown by the restoration of the normal $^{1}H,^{15}N$-HSQC fingerprint of the native protein (Fig. S6, *A and B*). Based on the high sequence and structural similarity, such high stability is likely typical for all the MBDs of ATP7A and ATP7B. In contrast, HMA1A displayed much more complex temperature-dependent dynamics with the reporter groups in various elements of the secondary structure showing different temperature-dependent transitions in the range 310–320 K (37–47°C), with a nearly complete protein unfolding at 323 K (50°C) (Fig. 5 *D*). Although no visible precipitation was observed, upon cooling the sample back to 298 K, the NMR spectrum showed only a few signals, indicating a disordered and aggregated protein (Fig. S6, *C and D*). Thus, HMA1A is quite unstable and may easily unfold at the physiological temperature of 37°C. Because, at ∼500 copies per cell, ATP7A is a very low abundance protein (49), HMA1A self-aggregation observed *in vitro* is unlikely to happen in the cell, and HMA1A unfolding may well be reversible in the intracellular environment. Stability and folding behavior of HMA1A may also be affected by the neighboring MBDs. In the previous NMR study of the complete MBD1–6 chain from ATP7A (18), backbone chemical shifts of most amino acid residues belonging to HMA1A were not assigned, possibly indicating complex dynamics of this domain in the MBD1–6 context.

The marginal stability of HMA1A suggests its possible role in modulating dynamic interactions between MBD1, MBD2, and MBD3. In ATP7B, MBD1–3 associate with each other in the copper-free form, but copper transfer from ATOX1-Cu breaks up the domain-domain interactions, an observation that led us to a model of ATP7B regulation through copper-dependent MBD dynamics (22,11). The length of the segment connecting MBD1 and MBD2 in ATP7A and ATP7B is very different, which should result

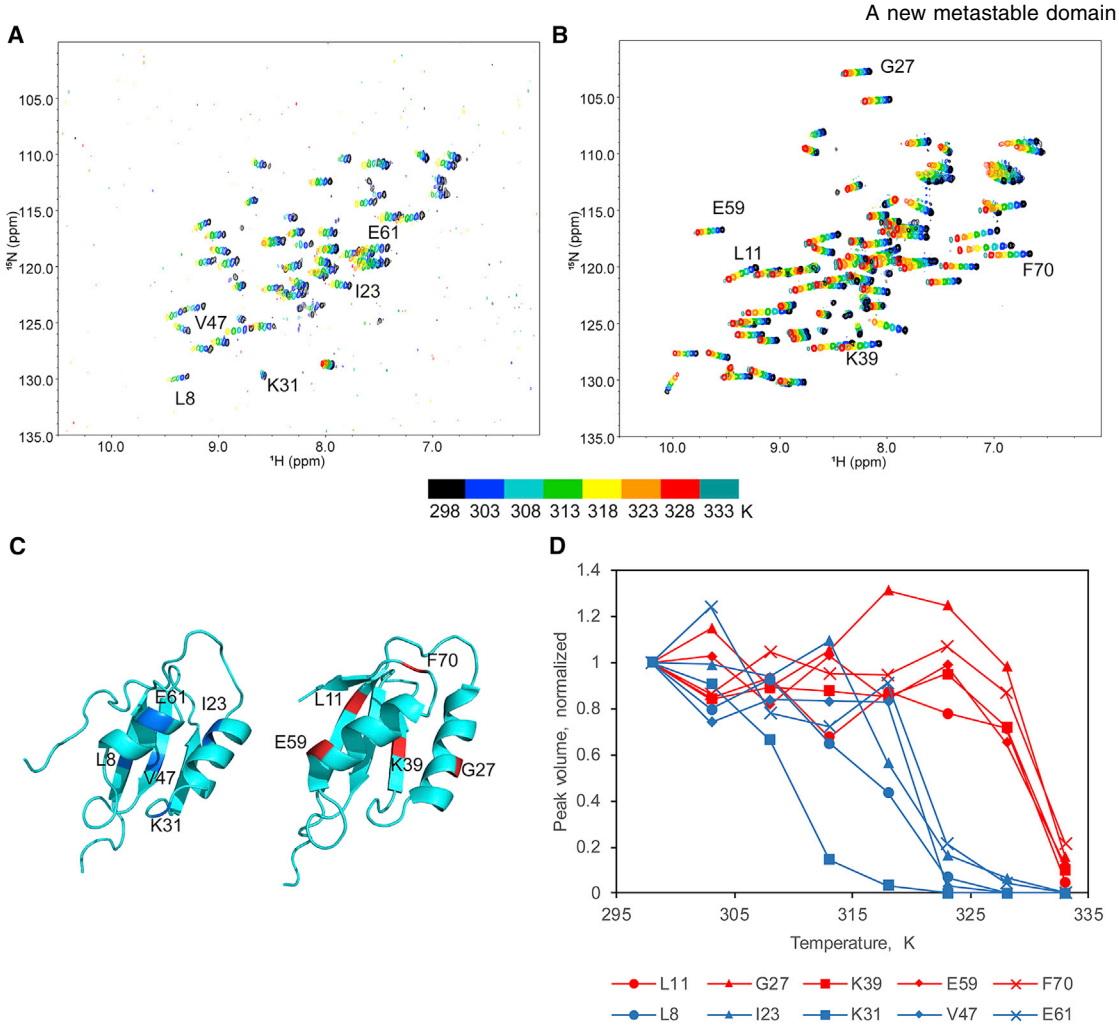

FIGURE 5 Low stability of HMA1A revealed by thermal denaturation. (*A* and *B*) The ^{1}H,^{15}N-HSQC spectra of HMA1A (*A*) and MBD2 of ATP7B (*B*) recorded at increasing temperatures, as shown by the color ramp below. (*C*) Location of the reporter backbone amide groups in the structures of HMA1A (*blue*) and MBD2 (*red*). The reporter amino acid residues are labeled. Residue numbering corresponds to the PDB deposited coordinate files. (*D*) Thermal denaturation curves of HMA1A (*blue*) and MBD2 (*red*) measured by the volumes of the backbone amide peaks of the reporter residues in the folded form. To see the figure in color, go online.

in different dynamics of MBD1–3 domain groups in these two proteins and may affect domain-domain interactions within the group. Another structural feature related to the mechanism of regulation is the disordered N-terminal peptide, which precedes MBD1 in ATP7B (ATP7B$_{1–63}$) but is completely absent from ATP7A, where MBD1 starts at the very N-terminus. The ATP7B$_{1–63}$ peptide was shown to interact with the N-domain and was implicated in the regulation of ATP7B activity and trafficking (11,50,51). These structural differences, along with the distinct functional roles and distinct cell and tissue distribution of ATP7A and ATP7B, suggest significant differences in the molecular mechanism of regulation between these two proteins. Yet, conservation in the sequence, structure, and the number of the MBDs indicates that this mechanism shares some fundamental features, such as the crucial role of domain-domain interactions in the MBD1–3 group.

We hypothesize that MBD1–3 interactions in ATP7A are modulated by the reversible folding-unfolding of the HMA1A domain. Because there are no copper-binding sites in HMA1A and it does not interact with either ATOX1 or ATOX1-Cu, HMA1A folding state cannot be directly regulated by copper. However, there are two kinase phosphorylation sites in HMA1A, S147 and T152. The T152 residue, in particular, appears to be phosphorylated in a copper-dependent manner (52). Phosphorylation of T152, and perhaps S147 in the presence of copper could facilitate unfolding of HMA1A, increasing MBD1-MBD2 freedom of motion and, consequently, promoting dissociation of the MBD1–3 domain group (Fig. 6).

CONCLUSIONS

We have described, to our knowledge, a new metastable folded domain in the region between the MBD1 and -2 of ATP7A, revealing a remarkable difference in the domain composition between the two copper-transporting ATPases in human cells. The structure of this domain, HMA1A,

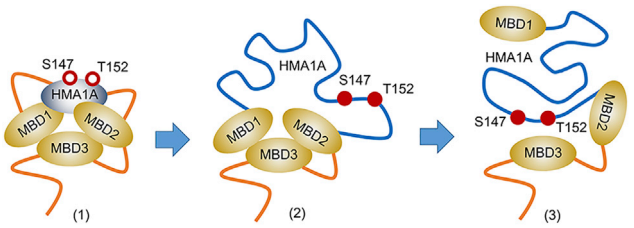

FIGURE 6 Proposed mechanism of ATP7A regulation by the reversible unfolding of the HMA1A domain. MBD1–3 associate in the inhibited state of the enzyme, by analogy with ATP7B (11). This association is stabilized by the folded HMA1A (*1*). Increased copper level in the cell leads to HMA1A unfolding, possibly via kinase signaling resulting in the phosphorylation on T152, and, perhaps, S147 (*2*). HMA1A unfolding, in turn, destabilizes MBD1–MBD3 interaction, leading to MBD1–3 domain group dissociation and, consequently, to the enzyme activation (*3*). To see the figure in color, go online.

resembles the MBDs but lacks the copper-binding site. We show that HMA1A is present in ATP7A proteins across evolutionary distant vertebrate species. We hypothesize that reversible unfolding of HMA1A is part of the mechanism of regulation of ATP7A through the copper-dependent dynamics and interactions of the MBDs.

SUPPORTING MATERIAL

Supporting material can be found online at https://doi.org/10.1016/j.bpj.2021.08.029.

AUTHOR CONTRIBUTIONS

Conceptualization was performed by O.Y.D.; methodology by E.-M.E.U., W.L., and M.T.; investigation by E.-M.E.U., W.L., M.T., and O.Y.D.; writing, original draft, by O.Y.D. and W.L.; writing, review and editing, by E.-M.E.U., W.L., M.T., and O.Y.D.; funding acquisition by O.Y.D.; and software by W.L.

ACKNOWLEDGMENTS

This work was supported by the Natural Sciences and Engineering Research Council of Canada Discovery grant RGPIN-2017-06822 to O.Y.D. NMR data were collected at the National Magnetic Resonance at Madison, which is supported by National Institutes of Health grant P41 GM103399 and by the University of Wisconsin–Madison, and at the Saskatchewan Structural Sciences Center at the University of Saskatchewan.

REFERENCES

1. Festa, R. A., and D. J. Thiele. 2011. Copper: an essential metal in biology. *Curr. Biol.* 21:R877–R883.
2. Gourdon, P., X. Y. Liu, …, P. Nissen. 2011. Crystal structure of a copper-transporting PIB-type ATPase. *Nature.* 475:59–64.
3. Lutsenko, S., N. L. Barnes, …, O. Y. Dmitriev. 2007. Function and regulation of human copper-transporting ATPases. *Physiol. Rev.* 87:1011–1046.
4. Morth, J. P., B. P. Pedersen, …, P. Nissen. 2007. Crystal structure of the sodium-potassium pump. *Nature.* 450:1043–1049.
5. Petrukhin, K., S. Lutsenko, …, T. C. Gilliam. 1994. Characterization of the Wilson disease gene encoding a P-type copper transporting ATPase: genomic organization, alternative splicing, and structure/function predictions. *Hum. Mol. Genet.* 3:1647–1656.
6. Schushan, M., A. Bhattacharjee, …, S. Lutsenko. 2012. A structural model of the copper ATPase ATP7B to facilitate analysis of Wilson disease-causing mutations and studies of the transport mechanism. *Metallomics.* 4:669–678.
7. Toyoshima, C., M. Nakasako, …, H. Ogawa. 2000. Crystal structure of the calcium pump of sarcoplasmic reticulum at 2.6 A resolution. *Nature.* 405:647–655.
8. Toyoshima, C., and G. Inesi. 2004. Structural basis of ion pumping by Ca2+-ATPase of the sarcoplasmic reticulum. *Annu. Rev. Biochem.* 73:269–292.
9. Arnesano, F., L. Banci, …, T. V. O'Halloran. 2002. Metallochaperones and metal-transporting ATPases: a comparative analysis of sequences and structures. *Genome Res.* 12:255–271.
10. Wernimont, A. K., D. L. Huffman, …, A. C. Rosenzweig. 2000. Structural basis for copper transfer by the metallochaperone for the Menkes/Wilson disease proteins. *Nat. Struct. Biol.* 7:766–771.
11. Yu, C. H., N. Yang, …, O. Y. Dmitriev. 2017. The metal chaperone Atox1 regulates the activity of the human copper transporter ATP7B by modulating domain dynamics. *J. Biol. Chem.* 292:18169–18177.
12. Linz, R., and S. Lutsenko. 2007. Copper-transporting ATPases ATP7A and ATP7B: cousins, not twins. *J. Bioenerg. Biomembr.* 39:403–407.
13. La Fontaine, S., and J. F. Mercer. 2007. Trafficking of the copper-ATPases, ATP7A and ATP7B: role in copper homeostasis. *Arch. Biochem. Biophys.* 463:149–167.
14. Lutsenko, S., A. Gupta, …, V. Zuzel. 2008. Cellular multitasking: the dual role of human Cu-ATPases in cofactor delivery and intracellular copper balance. *Arch. Biochem. Biophys.* 476:22–32.
15. Cater, M. A., J. Forbes, …, J. F. Mercer. 2004. Intracellular trafficking of the human Wilson protein: the role of the six N-terminal metal-binding sites. *Biochem. J.* 380:805–813.
16. Shanmugavel, K. P., and P. Wittung-Stafshede. 2019. Copper relay path through the N-terminus of Wilson disease protein, ATP7B. *Metallomics.* 11:1472–1480.
17. Huster, D., and S. Lutsenko. 2003. The distinct roles of the N-terminal copper-binding sites in regulation of catalytic activity of the Wilson's disease protein. *J. Biol. Chem.* 278:32212–32218.
18. Banci, L., I. Bertini, …, A. Rosato. 2007. The different intermolecular interactions of the soluble copper-binding domains of the menkes protein, ATP7A. *J. Biol. Chem.* 282:23140–23146.
19. Banci, L., I. Bertini, …, A. Rosato. 2009. An NMR study of the interaction of the N-terminal cytoplasmic tail of the Wilson disease protein with copper(I)-HAH1. *J. Biol. Chem.* 284:9354–9360.
20. Fatemi, N., D. M. Korzhnev, …, J. D. Forman-Kay. 2010. NMR characterization of copper-binding domains 4-6 of ATP7B. *Biochemistry.* 49:8468–8477.
21. Achila, D., L. Banci, …, D. L. Huffman. 2006. Structure of human Wilson protein domains 5 and 6 and their interplay with domain 4 and the copper chaperone HAH1 in copper uptake. *Proc. Natl. Acad. Sci. USA.* 103:5729–5734.
22. Huang, Y., S. Nokhrin, …, S. Lutsenko. 2014. Interactions between metal-binding domains modulate intracellular targeting of Cu(I)-ATPase ATP7B, as revealed by nanobody binding. *J. Biol. Chem.* 289:32682–32693.
23. Bartee, M. Y., M. Ralle, and S. Lutsenko. 2009. The loop connecting metal-binding domains 3 and 4 of ATP7B is a target of a kinase-mediated phosphorylation. *Biochemistry.* 48:5573–5581.
24. LeShane, E. S., U. Shinde, …, S. Lutsenko. 2010. Interactions between copper-binding sites determine the redox status and conformation of the regulatory N-terminal domain of ATP7B. *J. Biol. Chem.* 285:6327–6336.

25. Walker, J. M., D. Huster, …, S. Lutsenko. 2004. The N-terminal metal-binding site 2 of the Wilson's disease protein plays a key role in the transfer of copper from Atox1. *J. Biol. Chem.* 279:15376–15384.
26. Yatsunyk, L. A., and A. C. Rosenzweig. 2007. Cu(I) binding and transfer by the N terminus of the Wilson disease protein. *J. Biol. Chem.* 282:8622–8631.
27. Yu, C. H., N. V. Dolgova, and O. Y. Dmitriev. 2017. Dynamics of the metal binding domains and regulation of the human copper transporters ATP7B and ATP7A. *IUBMB Life.* 69:226–235.
28. de Castro, E., C. J. Sigrist, …, N. Hulo. 2006. ScanProsite: detection of PROSITE signature matches and ProRule-associated functional and structural residues in proteins. *Nucleic Acids Res.* 34:W362–W365.
29. Dmitriev, O., R. Tsivkovskii, …, S. Lutsenko. 2006. Solution structure of the N-domain of Wilson disease protein: distinct nucleotide-binding environment and effects of disease mutations. *Proc. Natl. Acad. Sci. USA.* 103:5302–5307.
30. Delaglio, F., S. Grzesiek, …, A. Bax. 1995. NMRPipe: a multidimensional spectral processing system based on UNIX pipes. *J. Biomol. NMR.* 6:277–293.
31. Ying, J., F. Delaglio, …, A. Bax. 2017. Sparse multidimensional iterative lineshape-enhanced (SMILE) reconstruction of both non-uniformly sampled and conventional NMR data. *J. Biomol. NMR.* 68:101–118.
32. Lee, W., M. Tonelli, and J. L. Markley. 2015. NMRFAM-SPARKY: enhanced software for biomolecular NMR spectroscopy. *Bioinformatics.* 31:1325–1327.
33. Shin, J., W. Lee, and W. Lee. 2008. Structural proteomics by NMR spectroscopy. *Expert Rev. Proteomics.* 5:589–601.
34. Lee, W., W. M. Westler, …, J. L. Markley. 2009. PINE-SPARKY: graphical interface for evaluating automated probabilistic peak assignments in protein NMR spectroscopy. *Bioinformatics.* 25:2085–2087.
35. Lee, W., A. Bahrami, …, J. L. Markley. 2019. I-PINE web server: an integrative probabilistic NMR assignment system for proteins. *J. Biomol. NMR.* 73:213–222.
36. Lee, W., J. L. Stark, and J. L. Markley. 2014. PONDEROSA-C/S: client-server based software package for automated protein 3D structure determination. *J. Biomol. NMR.* 60:73–75.
37. Lee, W., C. M. Petit, …, J. L. Markley. 2016. The AUDANA algorithm for automated protein 3D structure determination from NMR NOE data. *J. Biomol. NMR.* 65:51–57.
38. Lee, W., G. Cornilescu, …, J. L. Markley. 2016. Integrative NMR for biomolecular research. *J. Biomol. NMR.* 64:307–332.
39. Shen, Y., O. Lange, …, A. Bax. 2008. Consistent blind protein structure generation from NMR chemical shift data. *Proc. Natl. Acad. Sci. USA.* 105:4685–4690.
40. Schwieters, C. D., J. J. Kuszewski, …, G. M. Clore. 2003. The Xplor-NIH NMR molecular structure determination package. *J. Magn. Reson.* 160:65–73.
41. Frishman, D., and P. Argos. 1995. Knowledge-based protein secondary structure assignment. *Proteins.* 23:566–579.
42. Bhattacharya, A., R. Tejero, and G. T. Montelione. 2007. Evaluating protein structures determined by structural genomics consortia. *Proteins.* 66:778–795.
43. Berman, H., K. Henrick, …, J. L. Markley. 2007. The worldwide Protein Data Bank (wwPDB): ensuring a single, uniform archive of PDB data. *Nucleic Acids Res.* 35:D301–D303.
44. Ulrich, E. L., H. Akutsu, …, J. L. Markley. 2008. BioMagResBank. *Nucleic Acids Res.* 36:D402–D408.
45. Raman, S., R. Vernon, …, D. Baker. 2009. Structure prediction for CASP8 with all-atom refinement using Rosetta. *Proteins.* 77 (*Suppl* 9):89–99.
46. DeSilva, T. M., G. Veglia, and S. J. Opella. 2005. Solution structures of the reduced and Cu(I) bound forms of the first metal binding sequence of ATP7A associated with Menkes disease. *Proteins.* 61:1038–1049.
47. Banci, L., I. Bertini, …, A. Rosato. 2004. Solution structure and backbone dynamics of the Cu(I) and apo forms of the second metal-binding domain of the Menkes protein ATP7A. *Biochemistry.* 43:3396–3403.
48. Gupta, A., and S. Lutsenko. 2012. Evolution of copper transporting ATPases in eukaryotic organisms. *Curr. Genomics.* 13:124–133.
49. Beck, M., A. Schmidt, …, R. Aebersold. 2011. The quantitative proteome of a human cell line. *Mol. Syst. Biol.* 7:549.
50. Braiterman, L., L. Nyasae, …, A. Hubbard. 2009. Apical targeting and Golgi retention signals reside within a 9-amino acid sequence in the copper-ATPase, ATP7B. *Am. J. Physiol. Gastrointest. Liver Physiol.* 296:G433–G444.
51. Guo, Y., L. Nyasae, …, A. L. Hubbard. 2005. NH2-terminal signals in ATP7B Cu-ATPase mediate its Cu-dependent anterograde traffic in polarized hepatic cells. *Am. J. Physiol. Gastrointest. Liver Physiol.* 289:G904–G916.
52. Veldhuis, N. A., V. A. Valova, …, J. Camakaris. 2009. Phosphorylation regulates copper-responsive trafficking of the Menkes copper transporting P-type ATPase. *Int. J. Biochem. Cell Biol.* 41:2403–2412.